Original Article

Graphs Constructed from Instantaneous Amplitude and Phase of Electroencephalogram Successfully Differentiate Motor Imagery Tasks

Abstract

Background: Accurate classification of electroencephalogram (EEG) signals is challenging given the nonlinear and nonstationary nature of the data as well as subject-dependent variations. Graph signal processing (GSP) has shown promising results in the analysis of brain imaging data. **Methods:** In this article, a GSP-based approach is presented that exploits instantaneous amplitude and phase coupling between EEG time series to decode motor imagery (MI) tasks. A graph spectral representation of the Hilbert-transformed EEG signals is obtained, in which simultaneous diagonalization of covariance matrices provides the basis of a subspace that differentiates two classes of right hand and right foot MI tasks. To determine the most discriminative subspace, an exploratory analysis was conducted in the spectral domain of the graphs by ranking the graph frequency components using a feature selection method. The selected features are fed into a binary support vector machine that predicts the label of the test trials. **Results:** The performance of the proposed approach was evaluated on brain–computer interface competition III (IVa) dataset. **Conclusions:** Experimental results reflect that brain functional connectivity graphs derived using the instantaneous amplitude and phase of the EEG signals show comparable performance with the best results reported on these data in the literature, indicating the efficiency of the proposed method compared to the state-of-the-art methods.

Keywords: *Electroencephalogram, graph signal processing, Hilbert transform, instantaneous amplitude and phase, motor imagery decoding*

Submitted: 16-Oct-2024 **Revised:** 06-Dec-2024 **Accepted:** 30-Dec-2024 **Published:** 13-Mar-2025

Maliheh Miri[1], Vahid Abootalebi[1], Hamid Saeedi-Sourck[1], Dimitri Van De Ville[2,3], Hamid Behjat[4]

[1]Department of Electrical Engineering, Yazd University, Yazd, Iran, [2]Neuro-X Institute, EPFL, Geneva, Switzerland, [3]Department of Radiology and Medical Informatics, University of Geneva, Geneva, Switzerland, [4]Department of Biomedical Engineering, Lund University, Lund, Sweden

Introduction

Graph signal processing (GSP) is a recently emerged data analysis paradigm that enables applying signal processing techniques to data that reside on graphs.[1-3] A graph is a structure consisting of a set of vertices (nodes) that are connected by edges (links). In particular, GSP has shown promising results in the analysis of human brain functional magnetic resonance imaging,[4-6] for example, for enhanced brain activation mapping,[7] classification,[8,9] and dimensionality reduction.[10] More recently, by deriving the underlying graph structure embedded in electroencephalogram (EEG) data, GSP has provided the means for enhanced characterization of EEG signals.[11-14]

In contrast to their high temporal resolution in the range of milliseconds, EEG signals suffer from poor spatial resolution, which stems from two main factors: volume conduction effect of the head and low signal-to-noise ratio. Each EEG electrode records the electric field generated from millions of neurons, which get smeared during transmission from the source of activity to the scalp, known as volume conduction. Low spatial resolution of EEG signals sheds light on the importance of considering the latent spatial organization in these data. Graphs can be leveraged to unravel this hidden structure in EEG data and to extract spatial features. GSP techniques have been successfully utilized in denoising,[11] dimensionality reduction,[12] and motor imagery (MI) decoding[13,14] of EEG signals. In the study by Cattai *et al.*,[11] a GSP-based algorithm is proposed to address the problem of denoising common functional connectivity estimates to improve the detectability of different connectivity states. A dimensionality reduction method is proposed in the study by Tanaka *et al.*[12] for multiclass EEG classification. In this method, dimensionality reduction is

Address for correspondence:
Dr. Vahid Abootalebi, Department of Electrical Engineering, Yazd University, Yazd, Iran.
E-mail: abootalebi@yazd.ac.ir

Access this article online

Website: www.jmssjournal.net

DOI: 10.4103/jmss.jmss_63_24

Quick Response Code:

How to cite this article: Miri M, Abootalebi V, Saeedi-sourck H, Van De Ville D, Behjat H. Graphs constructed from instantaneous amplitude and phase of electroencephalogram successfully differentiate motor imagery tasks. J Med Signals Sens 2025;15:7.

achieved by spectral decomposition of a predefined brain graph. The brain graph is derived from a geometrical distribution of EEG electrodes. A novel GSP-based method on learned graphs is presented in the study by Miri *et al.*[13] for transforming EEG data into a spectral representation to extract spatial signal information from data. The applicability of the method was validated within the setting of classifying MI tasks.

Discrimination of dynamic states arising during the imagination of different motor tasks from EEG data is a challenging task in brain–computer interface (BCI) systems.[15,16] Many methods have been suggested in the literature for classifying MI-BCI tasks using EEG signals, focusing on features derived from the time, spatial, or frequency domains.[17-19] The use of wavelet transform, Riemannian geometry, transfer learning, and deep learning have been proposed for this purpose.[20-23] Although deep learning-based methods provide high classification accuracies, these approaches have two main drawbacks: the learning process of networks is time-consuming; moreover, these methods suffer from overfitting problem, especially for data with a small number of training trials in each class.

Typically, changes that appear in EEG data during MI tasks are measured by estimating the EEG signal power in specific frequency bands. However, the use of amplitude or phase information of EEG signals has also recently shown promising results in this application.[24,25] Considering that EEG signals are nonlinear and nonstationary, utilizing instantaneous amplitude or phase coupling between EEG time series enables a better understanding of the dynamic behavior of these signals. In the study by Huang *et al.*,[24] phase-locking value (PLV) and Phase-lag index (PLI) networks were combined with convolution neural networks for EEG motor movement/imagery classification. A method based on time–frequency-space pattern optimization was presented in the study by Liu *et al.*[25] that utilizes the Hilbert transform and common spatial patterns for MI EEG classification.

Inspired by the successful application of GSP in brain signal analysis, in this work, we propose a method for decoding MI tasks by deriving a graph representation from the instantaneous amplitude and phase of EEG signals. In the first step of the proposed method, a proper graph that captures the intrinsic underlying relation in the brain data should be defined. Consistent with prior related works,[13,14] we considered each electrode as a node of the graph. To obtain graph edges, we utilized four Hilbert transform-based functions to characterize the functional connectivity between EEG signals. In the next step, the brain data is mapped onto the Laplacian harmonics of the defined graphs. Then, the covariance matrix of the resulting spectral representations for each class of data is calculated. These covariance matrices are simultaneously diagonalized to form the basis of a subspace, in which two classes of MI tasks are maximally differentiated. To determine the most discriminative subspace, we explored the spectrum of the graphs by ranking the frequency components using a feature selection method. A binary support vector machine (SVM) was then trained using the selected features to predict the label of the test trials. Finally, the results obtained from the proposed method are compared to some state-of-the-art methods. The following sections of this article are structured as follows: Section "materials and methods" reviews the fundamental concepts and presents the proposed approach. Section "experimental results" elaborates on the results of the conducted experiments, and Section "discussion and conclusions" concludes with a discussion and final remarks.

Materials and Methods

Data

To conduct experiments and examine the performance of the proposed algorithm for classifying motor imagery tasks, publicly available EEG signals from BCI Competition III-Dataset IVa were used.[26] These signals were captured from five healthy individuals (labeled as aa, al, av, aw, and ay, respectively) with a sampling frequency of 100 Hz utilizing 118 electrodes organized according to the 10/20 system. Each subject was shown 280 visual cues for 3.5 s, providing 140 trials per class for right hand and right foot MI classes. According to the competition instruction, recorded trials have been divided into two sets of training and test data with different set sizes in each subject. For the first two subjects, aa and al, 60% and 80% of trials were labeled as training sets. For the other three subjects, av, aw, and ay, respectively, 30%, 20%, and 10% of the trials were considered as training sets. The rest of the trials in each subject were considered for the test sets.

Graph signal processing fundamentals

Let G = (V, E, **A**) represent an undirected, weighted graph, where V = {1, 2,…, N} refers to the N nodes (vertices) of the graph, E is the edge set (pairs [*i, j*] for $i, j \in V$), and **A** is the graph weighted adjacency matrix which is a symmetric matrix. To exploit the spectral properties of the graph, the graph Laplacian matrix is defined as **L = D-A**, where **D** is the degree matrix, i.e., $D_{ii} = \sum_j A_{ij}$. The symmetric normalized graph Laplacian is given as:

$$\boldsymbol{\mathcal{L}} = \boldsymbol{D}^{-1/2}\,\boldsymbol{L}\,\boldsymbol{D}^{-1/2} = \boldsymbol{I} - \boldsymbol{D}^{-1/2}\,\boldsymbol{A}\,\boldsymbol{D}^{-1/2}, \quad (1)$$

Where **I** indicates the identity matrix. Given that $\boldsymbol{\mathcal{L}}$ is positive semidefinite and real, it allows for eigen decomposition, represented as:

$$\boldsymbol{\mathcal{L}} = \mathbf{U}\Lambda\mathbf{U}^{T}, \quad (2)$$

where T indicates the transpose operator, $\mathbf{U} = \{\mathbf{u}_1, \mathbf{u}_2, \ldots, \mathbf{u}_N\}$ is the matrix of eigenvectors containing the orthonormal eigenvectors of $\boldsymbol{\mathcal{L}}$ in its columns, and $\boldsymbol{\Lambda}$ is a diagonal matrix that includes the corresponding eigenvalues $0 = \lambda_1 \le \lambda_2 \le \ldots \le \lambda_N \le 2$.

f is a graph signal that can be described as an N×1 vector. The n-th element of **f** reflects the signal value associated with node n in G. Graph signal **f** can be mapped onto the Laplacian eigenvectors and converted into a spectral representation called the graph Fourier transform (GFT) of **f**[2] as:

$$\hat{\mathbf{f}} = \mathbf{U}^{\mathbf{T}}\mathbf{f}. \tag{3}$$

The eigenvalues of the Laplacian matrix characterize the graph spectrum, while the associated eigenvectors provide an orthonormal basis that spans the graph spectral domain. Similar to the classical Fourier transform that encodes the temporal variation of signals, GFT encodes the spatial variability of graph signals. As such, graph Laplacian eigenvectors associated with higher eigenvalues capture a greater degree of spatial variability.[1,27] More explanation on GSP fundamentals is provided in supplementary information.

Graph representation of brain signals

In order to obtain a graph representation of brain signals, we defined subject-specific graphs by quantifying the functional connectivity between the signals acquired from electrodes. To compute the functional connectivity, we utilized the Hilbert transform of time courses. More precisely, the analytical form of signals is determined using the Hilbert transform as:

$$\mathbf{x}_{\mathrm{a}}(\mathrm{t}) = \mathbf{x}(\mathrm{t}) + \mathrm{j}\mathcal{H}\{\mathbf{x}(\mathrm{t})\} = A(\mathrm{t})\mathrm{e}^{\mathrm{j}\phi(\mathrm{t})} \tag{4}$$

Where **x**(t) is the signal located on an electrode, $\mathbf{x}_a$(t) is the analytical signal, and $\mathcal{H}\{\mathbf{x}(\mathrm{t})\}$ is the Hilbert transform of **x**(t) which is obtained as:

$$\mathcal{H}\{\mathbf{x}(t)\} = \frac{1}{\pi} PV \int_{-\infty}^{\infty} \frac{\mathbf{x}(\tau)}{t-\tau} d\tau, \tag{5}$$

Where *PV* is Cauchy Principal Value and *A*(t) and $\phi(\mathrm{t})$ in Eq. 4 indicate the instantaneous amplitude and phase of the signal, respectively. The amplitude and phase of the analytical signal is considered to obtain different types of functional connectivity. In this article, we utilized four types of Hilbert transform-based definitions of connectivity to define EEG graphs: one based on the amplitude and three based on the phase information. In the following, a description of these graphs is presented.

Amplitude envelope correlation

The amplitude envelope is defined as the absolute value of the Hilbert transform of the brain signal and reflects fluctuations in signal energy over time. Amplitude envelope correlation (AEC) is obtained by calculating the Pearson's correlation between the instantaneous amplitude of signals and computes the synchrony between the brain's functional networks. The range of AEC is between 0 and 1, with higher values indicating the synchronous fluctuations of amplitude envelopes.[28]

Phase-locking value

PLV calculates the time-varying phase difference between two signals as a measure of phase synchronization between the signals as:

$$PLV = \left| \mathrm{E}\left[e^{j\Delta\phi(t)} \right] \right|, \tag{6}$$

where $\Delta\phi(\mathrm{t})$ is the phase difference between two time points of the signal and E[.] denotes the expected value. The range of PLV is between 0 and 1 with 0 indicating no phase locking and 1 indicating complete phase locking.[29]

Phase-lag index

PLI is another measure that is used to quantify phase synchrony between the signals from different brain regions. The PLI provides information about the functional connectivity of the brain based on the stability of the phase difference between two signals. This measure is defined as:

$$PLI = \left| \mathrm{E}\left[sgn\left(\Delta\phi(t)\right) \right] \right|, \tag{7}$$

and is determined by calculating the average of the values obtained from the sign function applied to the difference of the instantaneous phase values of two signals, where sgn(.) denotes the sign function; note that PLI values fall within the continuous range [0 1]. Higher values of PLI indicate stronger phase synchronization between signals.[30]

Phase linearity measurement

This measure, which is a generalization of PLI, measures the synchrony of brain regions by observing their phase difference in time while accounting for small differences between the main frequency components of the signals. In particular, phase linearity measurement (PLM) calculates the percentage of spectral energy in a 2B narrow band centered at 0 in terms of the total signal energy.

$$PLM = \frac{\int_{-B}^{B} \left| \int_{0}^{T} e^{j\Delta\phi(t)} e^{-j2\pi ft}\, dt \right|^2 df}{\int_{-\infty}^{\infty} \left| \int_{0}^{T} e^{j\Delta\phi(t)} e^{-j2\pi ft}\, dt \right|^2 df}, \tag{8}$$

Where $\Delta\phi(\mathrm{t})$ is the phase difference between two time points of the signal, T is the number of time points located on each node of the graph, and B is considered to be 1 Hz by default.[31]

Proposed method

First, EEG graphs specific to each subject are extracted. By considering each subject's EEG data as graph signals, a spectral representation for the graph signals residing on these graphs is obtained by computing the GFT coefficients of the EEG signals. Then, to account for signal temporal dynamics, the FK transform has been used, which operates on the GFT coefficients and provides a discriminative subspace in the graph spectrum domain that can be employed to differentiate between two types of motor imagery tasks.[32] More precisely, by simultaneous diagonalization of covariance matrices of the GFT coefficients, a basis is obtained by mapping on which in one class, the variance of the signals is maximized, whereas for the other class, it is minimized. In this way, maximum differentiation between the classes of data is provided in a reduced dimension space. Finally, the variance of the representations mapped into this subspace is used as feature vectors to train and test the classifier.

Figure 1 provides a schematic representation of the proposed approach. Time points from 0.5 to 2.5 s after the visual cue for each trial were used to extract graph signals. Specifically, the EEG signal values across 118 electrodes per time instance were treated as one graph signal, resulting in 200 graph signals per trial. Given that motor imagery tasks modulate the mu and beta rhythms, EEG signals were filtered using a third-order Butterworth filter with a passband of 8–30 Hz.

To extract features for classification, we derived subject-specific graphs from the whole set of EEG trials at hand, using the methods described in the previous section. Let $\boldsymbol{F} = [\mathbf{f}_1,\ldots, \mathbf{f}_T]$ denote a set of graph signals at T time instances, where $\boldsymbol{X} = \boldsymbol{F}^T$ contains signals residing on the electrodes in its columns, such that $\mathbf{x}_i(t)$ is the signal residing on electrode *i,* for i = 1,…,118 and *t* = 1,…, T. By computing the analytical form of $\mathbf{x}_i$ (t) signals, the instantaneous amplitude and phase of the signals located on the electrodes were determined, which were used to obtain the AEC, PLV, PLI, and PLM graphs for each subject. Adjacency matrices and histogram of the Laplacian eigenvalues for the graphs of subject aa are presented in Figure 2. The eigenvectors of the normalized Laplacian matrix of each graph were utilized to compute the GFT coefficients for graph signals that have been demeaned and normalized. As such, a graph spectral representation of EEG signals was obtained. A representative subset of eigenvectors of the graphs derived for subject aa is shown in Figure 3.

The covariance matrix of the GFT coefficients for each class of data was then computed. In order to take into consideration the temporal information embedded in the EEG data, we used the FK transform, which simultaneously diagonalizes these two symmetric covariance matrices. This transform consists of three steps: whitening, simultaneous diagonalization, and finding the projection matrix. The projection matrix **W** maximizes the variance of EEG signals for one class while minimizing it for the other class. The **W** matrix was used to project the GFT coefficients to a discriminative feature space for two MI classes of right hand and right foot. More details and formulation of the FK transform are provided in Appendix 1 for interested readers. Then, the features extracted from this two-dimensional subspace were used for classification using a binary SVM classifier.

Experimental Results

As explained before, to obtain a graph representation of EEG signals, the methods described in section "graph representation of brain signals" were used. In our experiments for MI classification, the training set assigned to each subject was used to train the algorithms, and the performance of the proposed method was evaluated by determining the label of the trials belonging to the test set. In the first step, five different subsets of GFT coefficients were used to determine the mapping matrix and extract the feature vectors: all frequencies (AF), low frequencies (LF), medium frequencies (MF), and high frequencies (HF). This splitting was chosen as an initial coarse division of the spectrum, based on the prior works,[5,11] and was obtained by splitting the graph spectrum into three equal subbands. Concatenating the two subsets LF and HF provides the fifth subset, LF + HF.[11]

In the next step, these subsets of GFT coefficients are separately subjected to the FK transform to extract two

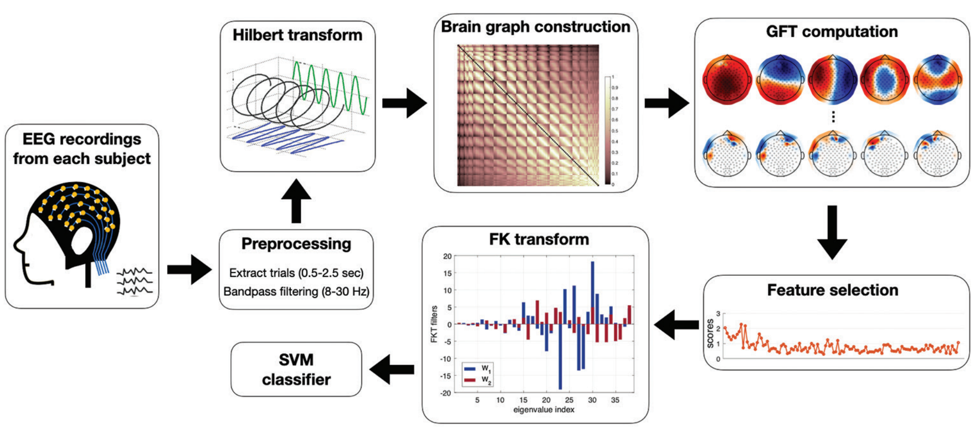

Figure 1: A schematic overview of the proposed method

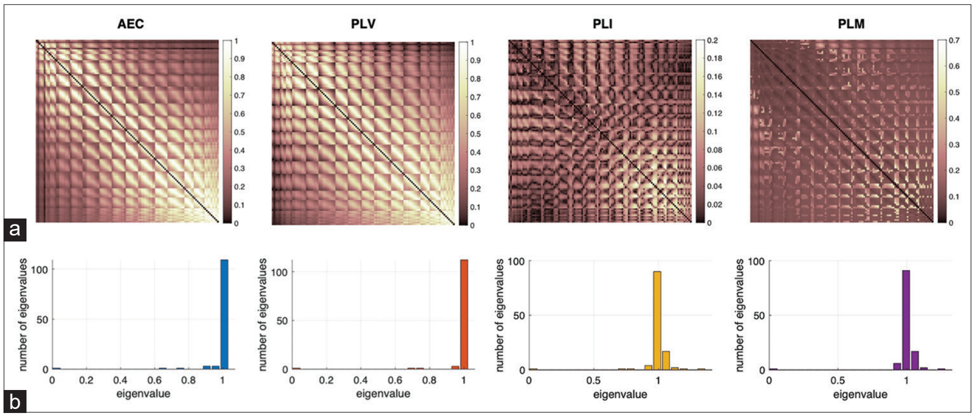

Figure 2: (a) Adjacency matrices of the graphs obtained for subject aa. (b) Histogram of the normalized Laplacian eigenvalues of the graphs shown in a

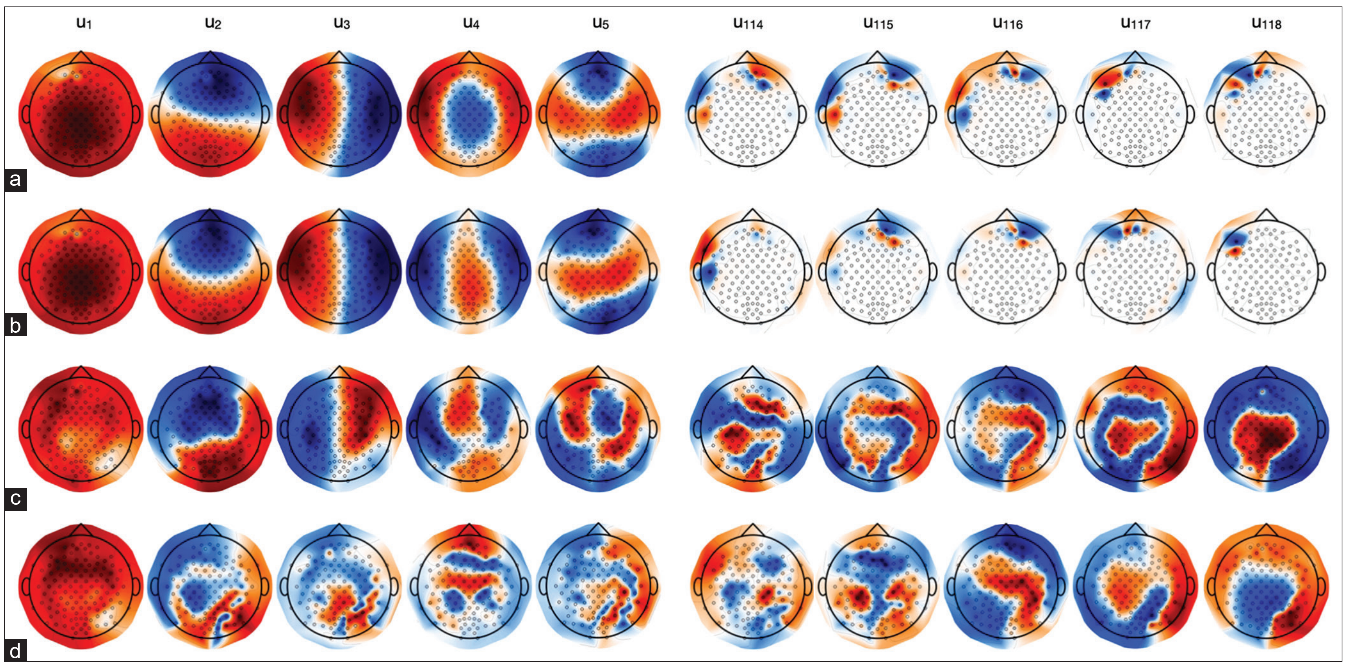

Figure 3: The first five and the last five eigenvectors of the amplitude envelope correlation (a), phase-locking value (b), phase-lag index (c), and phase linearity measurement (d) graphs derived for subject aa

discriminative filters placed in the rows of the mapping matrix **W**. The filters derived for subject aa using the four studied graphs are shown in Figure 4. Consequently, the logarithm of the variance of the GFT coefficients projected onto **W** provides features for classifying two MI tasks using SVM with linear kernel. SVM was selected because of its robustness and superior performance in BCI applications compared to other classifiers,[16] and low computational cost. Results of Using RBF Kernel in SVM is provided in supplementary information. Tables 1-4 show the classification performance achieved using four brain graphs for each subject separately, as well as the average across all subjects in five different frequency bands.

Across all graphs, classification performance achieved using the LF subset of the GFT coefficients notably outperforms the accuracy obtained using the MF and HF subsets which is consistent with previous studies.[12] Using both the AEC and PLV graphs, in four subjects and on average across all subjects, classification accuracy in the LF subband outperforms using the other subbands. For subject av, the best accuracy was obtained using all GFT coefficients. In the PLI and PLM graphs, the best accuracies are obtained in three of five subjects for both the AF and LF + HF subbands. In subject ay, LF coefficients resulted in the best accuracy. Moreover, classification accuracy on average across all subjects in the PLI and PLM graphs achieved the best result using the LF + HF subset. Overall, the best accuracy on average across all subjects was obtained using the PLV in the LF subband.

To identify the key features that are most effective for the classification of MI data, we used a feature selection algorithm that ranks the spectral graph components using the Wilcoxon statistical test. The logarithm of the variance of GFT coefficients was used as the input of

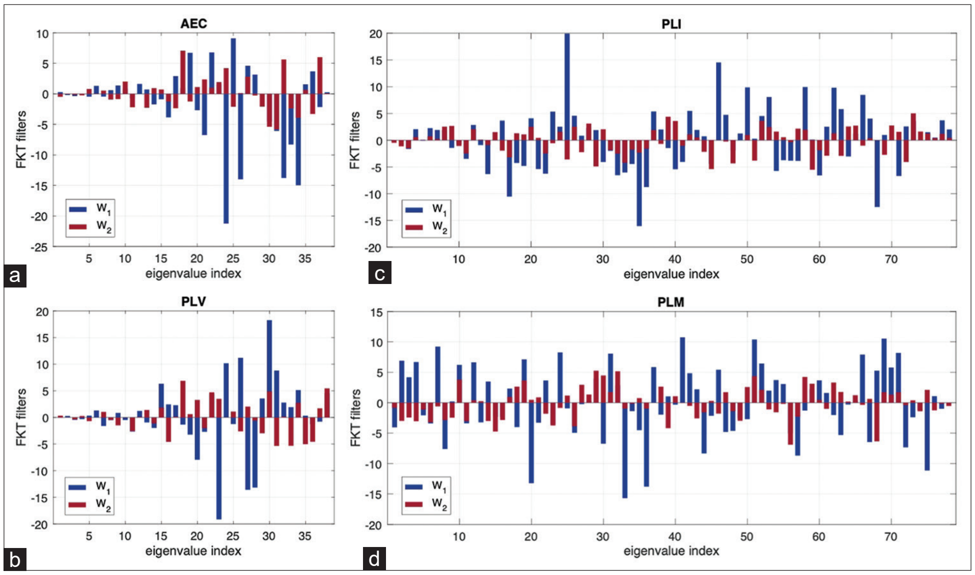

Figure 4: Filters extracted using FK transform for amplitude envelope correlation (a), phase-locking value (b), phase-lag index (c), and phase linearity measurement (d) graphs of subject aa

Table 1: Classification results (%) for the test sets using amplitude envelope correlation graphs

AEC	aa	al	av	aw	ay	Mean±SD
AF	71.43	100	69.90	87.95	72.62	80.38±13.16
LF	88.39	100	61.73	93.30	82.14	85.11±14.62
MF	63.39	66.07	49.49	58.93	52.38	58.05±7.05
HF	51.78	71.43	53.57	59.37	51.19	57.47±8.45
LF + HF	66.96	98.21	69.90	87.95	82.14	81.03±12.90

AF – All frequency; LF – Low frequency; HF – High frequency; AEC – Amplitude envelope correlation; SD – Standard deviation

Table 2: Classification results (%) for the test sets using phase-locking value graphs

PLV	aa	al	av	aw	ay	Mean±SD
AF	70.53	100	70.92	88.84	72.22	80.50±13.32
LF	83.03	100	67.86	91.96	83.73	85.32±11.96
MF	56.25	67.86	50.51	60.71	57.94	58.65±6.35
HF	56.25	71.43	52.04	55.80	46.03	56.31±9.40
LF + HF	66.96	100	70.41	91.07	82.94	82.28±13.85

PLV – Phase-locking value; AF – All frequency; LF – Low frequency; HF – High frequency; MF – Medium frequency; SD – Standard deviation

the rank features function in MATLAB, and the score of each feature was determined. More distinct features were assigned higher scores. The optimal number of top-ranked features selected for classification was determined using 10-fold cross-validation on the training sets in each subject. First, the classification accuracy was calculated using the selected features from the entire set of GFT coefficients, the results of which are presented in Table 5.

Figure 5 shows the scores of the GFT coefficients on average across subjects in each studied graph. In the AEC and PLV graphs, the highest scores are for GFT coefficients associated with eigenvalue in the lowest one-third of the

Table 3: Classification results (%) for the test sets using phase-lag index graphs

PLI	aa	al	av	aw	ay	Mean±SD
AF	75.00	100	71.43	90.62	71.82	81.77±12.87
LF	72.32	96.43	66.33	71.87	85.32	78.45±12.23
MF	64.28	80.36	58.16	58.48	71.03	66.46±9.37
HF	65.18	100	60.71	58.03	60.71	68.93±17.56
LF + HF	80.36	100	70.41	90.62	75.00	83.28±12.00

PLI – Phase-lag index; AF – All frequency; LF – Low frequency; HF – High frequency; SD – Standard deviation

Table 4: Classification results (%) for the test sets using phase linearity measurement graphs

PLM	aa	al	av	aw	ay	Mean±SD
AF	73.21	100	70.92	90.62	70.63	81.08±13.45
LF	70.53	98.21	60.71	56.25	84.52	74.05±17.32
MF	68.75	82.14	53.57	87.95	50.40	68.56±16.70
HF	65.18	98.21	68.88	59.82	71.43	72.70±14.91
LF + HF	80.36	100	70.92	79.91	80.16	82.27±10.69

PLM – Phase linearity measurement; AF – All frequency; LF – Low frequency; HF – High frequency; SD – Standard deviation

Table 5: Classification results (%) for the test sets using features selected from all frequency bands

Graph	aa	al	av	aw	ay	Mean±SD
AEC	75.89	100	71.94	87.95	82.54	83.66±11.00
PLV	79.46	100	70.92	90.18	84.13	84.94±10.97
PLI	78.57	100	71.94	92.41	85.32	85.65±11.07
PLM	79.46	100	72.96	92.41	88.49	86.66±10.65

PLM – Phase linearity measurement; PLI – Phase-lag index; PLV – Phase-locking value; AEC – Amplitude envelope correlation; SD – Standard deviation

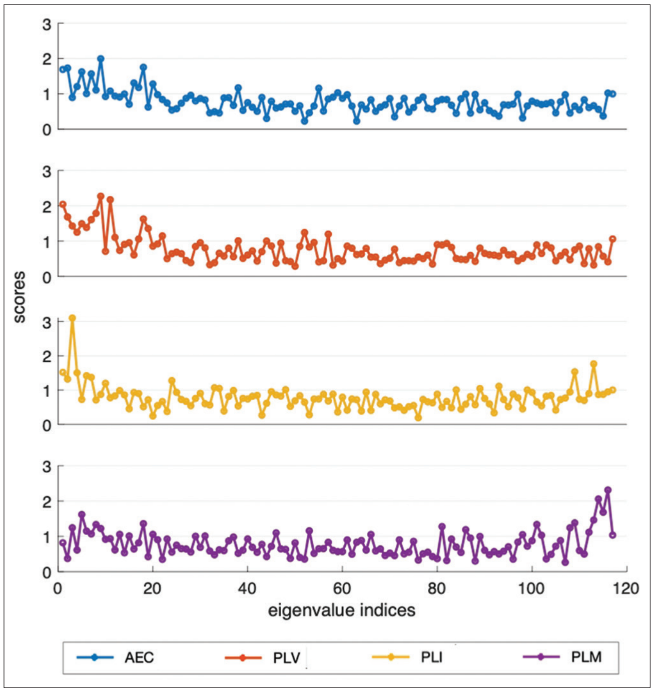

Figure 5: Scores of graph frequencies on average across five subjects in each graph

spectrum, while in the PLI, and especially in the PLM graphs, there are also high scores in the HF subband.

Considering the substantial classification accuracy resulting from the use of the LF subset of GFT coefficients in the AEC and PLV graphs, we attempted to specify the most discriminative features in this subband instead of on the entire spectrum. We repeated the same procedure for the PLI and PLM graphs, and the test set trials were classified using the selected features in the LF + HF subband. Classification results obtained from this analysis are shown in Table 6. Overall, the highest performance on average across subjects was achieved in the AEC graph using the features selected from the LF subband.

Finally, classification results obtained by the proposed method are compared with some state-of-the-art techniques in Table 7. Among conventional studies conducted on these data, we considered those methods for comparison that use the same settings and data divisions as our proposed approach to classify MI tasks. More precisely, in these methods, the number of trials in the train and test sets of each subject as well as the preprocessing steps are completely in accordance with what we have considered in the present work. Two of these methods are based on GSP (GL and GSL), and the other two use generalizations of FK transform (RCSSP and BECSP). The performance of our method, which uses a simple analytical definition of graphs based on the Hilbert transform of EEG data, is on par with the GL method that uses a graph structure learning approach to derive graphs from raw EEG data, both outperform the other three methods.

Table 6: Classification results (%) for the test sets using features selected from the low frequencies subband for amplitude envelope correlation and phase-locking value, and the low frequencies + high frequencies subband for phase-lag index and phase linearity measurement

Graph	aa	Al	av	aw	ay	Mean±SD
AEC (LF)	88.39	100	71.43	94.20	87.70	88.34±10.68
PLV (LF)	85.71	100	69.90	92.41	85.71	86.75±11.11
PLI (LF + HF)	82.14	100	70.92	91.52	87.30	86.38±10.84
PLM (LF + HF)	77.68	100	73.98	86.16	87.30	85.02±10.08

PLM – Phase linearity measurement; PLI – Phase-lag index; PLV – Phase-locking value; AEC – Amplitude envelope correlation; SD – Standard deviation; LF – Low frequency; HF – High frequency

Table 7: Comparing the performance of the proposed method with some alternative methods

Method	aa	al	av	aw	ay	Mean±SD
Proposed	88.39	100	71.43	94.20	87.70	88.34±10.68
GL[13]	87.50	100	70.92	91.96	92.86	88.65±10.88
GSL[33]	85.71	98.21	75.00	85.27	90.48	86.93±8.46
RCSSP[34]	82.14	96.42	68.87	98.21	88.88	86.91±11.94
BECSP[35]	77.68	100	73.98	84.82	88.10	84.91±10.12

SD – Standard deviation; GL: Graph learning, GSL: Graph structure learning, RCSSP: Regularized common spatio-spectral pattern, BECSP: Bispectrum, entropy and common spatial pattern

Discussion and Conclusions

This article presents a graph representation-based framework for classifying motor imagery tasks from EEG data. Experimental results reflect that brain functional connectivity graphs derived using the instantaneous amplitude and phase of the EEG signals show comparable performance with the best results reported on these data in the literature. Even though methods based on deep learning show promising results,[36] they are resource-intensive and therefore not a good option for individualized MI task decoding or neurofeedback applications. Moreover, GSP is advantageous over deep learning methods as it provides a means to link MI task decoding to a generating basis that can be used to break down EEG signals into interpretable subcomponents based on their contribution and significance for MI task decoding. Although the average accuracy across all subjects reported by the GL method is slightly higher than the average accuracy obtained by the proposed method, the proposed method outperforms the GL approach in three of five subjects. Only for subject ay, which has the smallest training set size, the proposed method shows lower accuracy compared to the GL method. It is worth noting that there is no need to learn the graphs in the proposed method; as such, the complex computations required for the optimization process are avoided.

Our results show that mapping the brain signals onto a low-dimensional subspace derived from the graph Fourier components strongly differentiates two classes of MI. Moreover, overfitting to the training data is avoided, which is especially important for subjects with small sizes of training data. Furthermore, our results confirm that incorporating temporal information with functional brain connectivity derived using the studied graph representations enhances the performance of the EEG signals classification in the proposed approach.

Results presented in Tables 5 and 6 show that, on average across all subjects, simultaneous diagonalization of covariance matrices computed from a selected subset of GFT coefficients yields a more differentiating subspace than employing frequency elements across the entire spectrum of the analyzed graphs, except for the PLM; in PLM, the energy of EEG graph signals is spread more broadly across the graph spectra for three of the five subjects (aa, aw, and ay); however, in subject av, using features selected from the entire set of graph frequencies deteriorates the classification performance.

Despite the identical results obtained for subject al in all the graphs [Tables 5 and 6] that indicate saturated performance, using a subband of the graph spectrum reduces the performance of the method for subject av in the first three graphs and for subject aw in the PLI graph. These results reflect the potential benefits of a subject-specific definition of the appropriate subband for feature selection. Overall, the highest average accuracy was attained by leveraging only the features selected from the lower one-third of graph frequencies in the AEC graphs.

The energy profiles of EEG graph signals for subjects aa and ay, are more localized to a subband of the graph spectrum that represents sparse or bandlimited graph signals [Tables 1-4]. On the contrary, for subjects al and av, the energy of signals is more broadly spread over the entire spectrum of the studied graphs. However, subject aw shows a more localized pattern in its energy profile for the AEC and PLV graphs compared to the PLI and PLM graphs.

Prior work suggests that information that explains brain activity is carried by both anatomically aligned and liberal components embedded in graph signals.[4] Considering that the eigenvalues of the normalized Laplacian matrix of the graphs are the basis of the graph frequency domain, graph signals are said to be aligned or smooth with the underlying brain structure if most of their energy is concentrated in the lower end of the graph spectrum. On the other hand, the energy of the liberal or localized graph signals is mainly concentrated in the higher end of the graph spectra. Unlike the AEC and PLV graphs on which the brain graph signals are smooth, the PLI and PLM graphs provide a substrate where the EEG graph signals manifest both liberal and aligned components [Tables 1-4].

As previously mentioned, spatial leakage of activity-induced electric fields, also known as volume conduction, leads to low spatial resolution of EEG data. Among the studied brain graphs, the AEC and PLV are susceptible to volume conduction. However, the PLI is insensitive to volume conduction because it excludes zero-phase lag interactions between EEG electrodes. The PLM formulation also includes a correction for volume conduction by removing phase difference components < 0.1 Hz.[31] It seems that the correction of volume conduction reflects better accuracies for the MI task classification using the GFT elements distributed across the graph spectra, compared to utilizing the graph frequency coefficients from the LF subband. Although correction of the volume conduction can be useful in some applications, it does not show any significant improvement in MI task decoding from EEG signals. It can be interpreted as a reduction in the inherent spatial smoothness of EEG signals by removing volume conduction. However, our analysis showed that MI tasks can be effectively decoded using only the lower subset of the graph frequency components, reinforcing the hypothesis that imagined motor activities are generally spatially smooth on brain graphs.[13]

Inspired by the promising results of using graph learning techniques in MI decoding,[13] in future work, we will explore alternative techniques for inferring brain graphs from EEG data by combining the instantaneous amplitude/phase of the signals and graph structure learning frameworks.[37] The proposed approach can be easily adapted to other imaging modalities such as MEG data. It can be interesting to further extend the proposed method to other phase-based measures, apart from the ones we validated in this study, such as the modulation index,[38] which is based on a normalized entropy measure and detect phase-amplitude coupling and could offer a more comprehensive view of cross-frequency interactions. Considering that the studied brain graphs are subject specific, they can be used in online applications such as neurofeedback. Utilizing the derived graphs for fingerprinting applications would also be an intriguing avenue for future research. In the studies by Miri *et al.* and Miri *et al.*,[39,40] the effectiveness of the graphs learned from the amplitude of EEG signals in characterizing an individual is shown. The potential of using phase-based EEG graphs in identifying individuals should be investigated in future. Moreover, these graphs can be derived from resting-state EEG data to tap into understanding individual differences in cortical functional organization in health and disease. We will also direct our future efforts toward utilizing FK transform extensions to generalize the proposed approach to decoding multiclass EEG tasks.

Acknowledgments

This research study was conducted retrospectively using publicly available human subject data from the Berlin BCI group. Our local ethics committee has determined that ethical approval is not necessary for analyzing this openly accessible data.

Financial support and sponsorship

Nil.

Conflicts of interest

There are no conflicts of interest.

References

1. Ortega A, Frossard P, Kovačević J, Moura JM, Vandergheynst P. Graph signal processing: Overview, challenges, and applications. Proc IEEE 2018;106:808-28.
2. Shuman DI, Narang SK, Frossard P, Ortega A, Vandergheynst P. The emerging field of signal processing on graphs: Extending high-dimensional data analysis to networks and other irregular domains. IEEE Signal Process Mag 2013;30:83-98.
3. Stanković L, Mandic D, Daković M, Scalzo B, Brajović M, Sejdić E, *et al*. Vertex-frequency graph signal processing: A comprehensive review. Digit Signal Process 2020;107:102802.
4. Huang W, Bolton TA, Medaglia JD, Bassett DS, Ribeiro A, Van De Ville D. A graph signal processing perspective on functional brain imaging. Proc IEEE 2018;106:868-85.
5. Medaglia JD, Huang W, Karuza EA, Kelkar A, Thompson-Schill SL, Ribeiro A, *et al.* Functional alignment with anatomical networks is associated with cognitive flexibility. Nat Hum Behav 2018;2:156-64.
6. Rué-Queralt J, Fluhr H, Tourbier S, Aleman-Gómez Y, Pascucci D, Yerly J, *et al.* Connectome spectrum electromagnetic tomography: A method to reconstruct electrical brain source networks at high-spatial resolution. Hum Brain Mapp 2024;45:e26638.
7. Abramian D, Larsson M, Eklund A, Aganj I, Westin CF, Behjat H. Diffusion-informed spatial smoothing of fMRI data in white matter using spectral graph filters. Neuroimage 2021;237:118095.
8. Griffa A, Amico E, Liégeois R, Van De Ville D, Preti MG. Brain structure-function coupling provides signatures for task decoding and individual fingerprinting. Neuroimage 2022;250:118970.
9. Itani S, Thanou D. Combining anatomical and functional networks for neuropathology identification: A case study on autism spectrum disorder. Med Image Anal 2021;69:101986.
10. Behjat H, Tarun A, Abramian D, Larsson M, Van De Ville D. Voxel-wise brain graphs from diffusion MRI: Intrinsic eigenspace dimensionality and application to functional MRI. IEEE Open J Eng Med Biol 2023.
11. Cattai T, Scarano G, Corsi MC, Bassett DS, Fallani FD, Colonnese S. Improving J-divergence of brain connectivity states by graph laplacian denoising. Trans Signal Inf Process Netw 2021;7:493-508.
12. Tanaka T, Uehara T, Tanaka Y. Dimensionality reduction of sample covariance matrices by graph Fourier transform for motor imagery brain-machine interface. In: 2016 IEEE Statistical Signal Processing Workshop (SSP). IEEE; 2016. p. 1-5.
13. Miri M, Abootalebi V, Saeedi-Sourck H, Van De Ville D, Behjat H. Spectral representation of EEG data using learned graphs with application to motor imagery decoding. Biomed Signal Process Control 2024;87:105537.
14. Miri M, Abootalebi V, Behjat H. Enhanced motor imagery-based EEG classification using a discriminative graph Fourier subspace. In: 2022 IEEE 19th International Symposium on Biomedical Imaging (ISBI). IEEE; 2022. p. 1-5.
15. Singh A, Hussain AA, Lal S, Guesgen HW. A comprehensive review on critical issues and possible solutions of motor imagery based electroencephalography brain-computer interface. Sensors (Basel) 2021;21:2173.
16. Lotte F, Bougrain L, Cichocki A, Clerc M, Congedo M, Rakotomamonjy A, *et al*. A review of classification algorithms for EEG-based brain-computer interfaces: A 10 year update. J Neural Eng 2018;15:031005.
17. Lee SB, Kim HJ, Kim H, Jeong JH, Lee SW, Kim DJ. Comparative analysis of features extracted from EEG spatial, spectral and temporal domains for binary and multiclass motor imagery classification. Inf Sci 2019;502:190-200.
18. Mohammadi E, Daneshmand PG, Khorzooghi SM. Electroencephalography-based brain-computer interface motor imagery classification. J Med Signals Sens 2022;12:40-7.
19. Seifzadeh S, Rezaei M, Faez K, Amiri M. Fast and efficient four-class motor imagery electroencephalography signal analysis using common spatial pattern-ridge regression algorithm for the purpose of brain-computer interface. J Med Signals Sens 2017;7:80-5.
20. Hu D, Li W, Chen X. Feature extraction of motor imagery EEG signals based on wavelet packet decomposition. In: The 2011 IEEE/ICME International Conference on Complex Medical Engineering. IEEE; 2011. p. 694-7.
21. Barachant A, Bonnet S, Congedo M, Jutten C. Multiclass brain-computer interface classification by Riemannian geometry. IEEE Trans Biomed Eng 2011;59:920-8.
22. Peterson V, Nieto N, Wyser D, Lambercy O, Gassert R, Milone DH, *et al.* Transfer learning based on optimal transport for motor imagery brain-computer interfaces. IEEE Trans Biomed Eng 2022;69:807-17.
23. Dose H, Møller JS, Iversen HK, Puthusserypady S. An end-to-end deep learning approach to MI-EEG signal classification for BCIs. Expert Syst Appl 2018;114:532-42.
24. Huang W, Chang W, Yan G, Zhang Y, Yuan Y. Spatio-spectral feature classification combining 3D-convolutional neural networks with long short-term memory for motor movement/imagery. Eng Appl Artif Intell 2023;120:105862.
25. Liu X, Sun Y, Zheng D, Na R. Hilbert-Huang transformation-based subject-specific time-frequency-space pattern optimization for motor imagery electroencephalogram classification. Measurement 2023;223:113673.
26. Blankertz B, Müller KR, Krusienski DJ, Schalk G, Wolpaw JR, Schlögl A, *et al.* The BCI competition. III: Validating alternative approaches to actual BCI problems. IEEE Trans Neural Syst Rehabil Eng 2006;14:153-9.
27. Shuman DI, Ricaud B, Vandergheynst P. Vertex-frequency analysis on graphs. Appl Comput Harmon Anal 2016;40:260-91.
28. Bruns A, Eckhorn R, Jokeit H, Ebner A. Amplitude envelope correlation detects coupling among incoherent brain signals. Neuroreport 2000;11:1509-14.
29. Lachaux JP, Rodriguez E, Martinerie J, Varela FJ. Measuring phase synchrony in brain signals. Hum Brain Mapp 1999;8:194-208.
30. Stam CJ, Nolte G, Daffertshofer A. Phase lag index: Assessment of functional connectivity from multi channel EEG and MEG with diminished bias from common sources. Hum Brain Mapp 2007;28:1178-93.
31. Baselice F, Sorriso A, Rucco R, Sorrentino P. Phase linearity measurement: A novel index for brain functional connectivity. IEEE Trans Med Imaging 2019;38:873-82.
32. Fukunaga K. Introduction to Statistical Pattern Recognition. Netherlands: Elsevier; 2013.
33. Georgiadis K, Adamos DA, Nikolopoulos S, Laskaris N, Kompatsiaris I. Covariation informed graph slepians for motor imagery decoding. IEEE Trans Neural Syst Rehabil Eng 2021;29:340-9.

34. Cherloo MN, Amiri HK, Daliri MR. Ensemble regularized common spatio-spectral pattern (ensemble RCSSP) model for motor imagery-based EEG signal classification. Comput Biol Med 2021;135:104546.
35. Hou Y, Chen T, Lun X, Wang F. A novel method for classification of multi-class motor imagery tasks based on feature fusion. Neurosci Res 2022;176:40-8.
36. Wang X, Liesaputra V, Liu Z, Wang Y, Huang Z. An in-depth survey on deep learning-based motor imagery electroencephalogram (EEG) classification. Artif Intell Med 2024;147:102738.
37. Kalofolias V. How to learn a graph from smooth signals. In Artificial intelligence and statistics. PMLR; 2016. p. 920-9.
38. Tort AB, Kramer MA, Thorn C, Gibson DJ, Kubota Y, Graybiel AM, *et al.* Dynamic cross-frequency couplings of local field potential oscillations in rat striatum and hippocampus during performance of a T-maze task. Proc Natl Acad Sci U S A 2008;105:20517-22.
39. Miri M, Abootalebi V, Amico E, Saeedi-Sourck H, Van De Ville D, Behjat H. Brain Fingerprinting Using EEG Graph Inference. In: 2023 31st European Signal Processing Conference (EUSIPCO). IEEE; 2023. p. 1025-9.
40. Miri M, Abootalebi V, Amico E, Saeedi-Sourck H, Van De Ville D, Behjat H. Graph learning from EEG data improves brain fingerprinting compared to correlation-based connectomes. Sci Talks 2024;10:100330.

Supplementary Information

Graph Signal Processing Fundamentals

A visual representation of the construction of brain graphs and the graph signals residing on these graphs is shown in Supplementary Figure 1. A representative graph consisting of six nodes (vertices) and eight edges is shown, where nodes represent EEG electrodes or different brain regions, and their relationship is described by the edges connecting them. Brain signals are considered as time series captured by each electrode. At any particular time point, the amplitude of the time series corresponds to the values of the graph signals on the nodes.[1]

Results of Using RBF Kernel in Support Vector Machine

Supplementary Tables 1 and 2 show the classification performance achieved using radial basis function (RBF) kernel (default values) in the SVM classifier for different graphs for each subject separately, as well as the average across all subjects in two different frequency bands (AF and LF).

Reference

1. Aviyente S, Villafañe-Delgado M. Graph signal processing on neuronal networks. In Cooperative and Graph Signal Processing: Academic Press; 2018. p. 799-816.

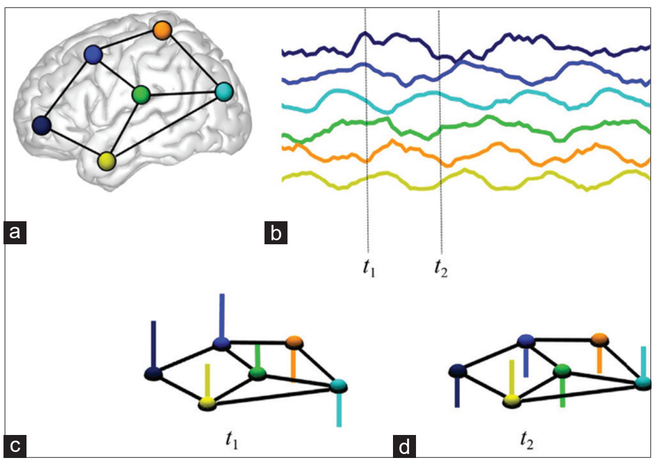

Supplementary Figure 1: An illustration of the graph's fundamental concepts. (a) A representative graph of the human brain. (b) Time series corresponding to each node in a. (c and d) Graph signals resided on the graphs at two different time points[1]

Supplementary Table 1: Classification results (%) for the test sets using support vector machine with radial basis function kernel in the all frequencies band

Graph	aa	al	av	aw	ay	Mean±SD
AEC	65.18	100	69.39	86.61	71.03	78.44±14.53
PLV	64.28	100	69.9	87.05	71.43	78.53±14.67
PLI	66.96	100	70.41	86.16	71.43	78.99±13.86
PLM	67.86	100	68.37	85.71	68.65	78.12±14.37

PLM – Phase linearity measurement; PLI – Phase-lag index; PLV – Phase-locking value; AEC – Amplitude envelope correlation; SD – Standard deviation

Supplementary Table 2: Classification results (%) for the test sets using support vector machine with radial basis function kernel in the low frequencies subband

Graph	aa	al	av	aw	ay	Mean±SD
AEC	72.32	96.43	58.67	94.20	86.11	81.55±15.9
PLV	67.86	100	62.24	91.96	82.94	81±15.87
PLI	68.75	96.43	62.24	57.59	81.35	73.27±15.73
PLM	69.64	94.64	54.08	59.37	83.73	72.29±16.85

PLM – Phase linearity measurement; PLI – Phase-lag index; PLV – Phase-locking value; AEC – Amplitude envelope correlation; SD – Standard deviation

Appendix

Appendix 1: FK Transform

Let $\mathbf{F}$ denote an N×T matrix containing graph signals from one trial in its columns and $\hat{\mathbf{F}}$ denote its related GFT matrix. The sample covariance matrices for each class are computed as:

$$\bar{\mathbf{C}}_i = \frac{1}{K_i}\sum_{k=1}^{K_i}\frac{\hat{\mathbf{F}}_{k,i}\hat{\mathbf{F}}_{k,i}^T}{tr(\hat{\mathbf{F}}_{k,i}\hat{\mathbf{F}}_{k,i}^T)}, \tag{1}$$

where tr(.) indicates the trace operator, and K_i refers to the number of trials assigned to class i. First, $\bar{\mathbf{C}} = \bar{\mathbf{C}}_1 + \bar{\mathbf{C}}_2$ should be whiten such that:

$$\mathbf{P}^T\bar{\mathbf{C}}\mathbf{P} = \mathbf{P}^T\left(\bar{\mathbf{C}}_1 + \bar{\mathbf{C}}_2\right)\mathbf{P} = \tilde{\mathbf{C}}_1 + \tilde{\mathbf{C}}_2 = \mathbf{I}, \tag{2}$$

where the whitening transform P can be obtained through the singular value decomposition of $\bar{\mathbf{C}}$ as follows:

$$\bar{\mathbf{C}} = \mathbf{QRQ}^T;\ \mathbf{P} = \frac{\mathbf{Q}}{\sqrt{\mathbf{R}}}. \tag{3}$$

In the next step, eigenvalue decomposition of $\tilde{\mathbf{C}}_1$ and $\tilde{\mathbf{C}}_2$ gives:

$$\begin{aligned}\tilde{\mathbf{C}}_1 &= \mathbf{DYD}^T\\ \tilde{\mathbf{C}}_2 &= \mathbf{D}(1-\mathbf{Y})\mathbf{D}^T\end{aligned}. \tag{4}$$

$\tilde{\mathbf{C}}_1$ and $\tilde{\mathbf{C}}_2$ exhibit the same eigenvectors, with complementary eigenvalues. Accordingly, the eigenvector that is associated with the smallest eigenvalue of $\tilde{\mathbf{C}}_1$ aligns with the largest eigenvalue of $\tilde{\mathbf{C}}_2$. The final transformation matrix is defined as:[32]

$$\mathbf{W} = \mathbf{D}^T\mathbf{P}. \tag{5}$$